

Characterization of Asymmetric Coplanar Waveguide Discontinuities

Nihad I. Dib, *Member, IEEE*, Mino Gupta, George E. Ponchak, *Member, IEEE*,
and Linda P. B. Katehi, *Senior Member, IEEE*

Abstract—A general technique to characterize asymmetric coplanar waveguide (CPW) discontinuities with air bridges where both the fundamental coplanar and slotline modes may be excited together is presented. First, the CPW discontinuity without air bridges is analyzed using the space-domain integral equation (SDIE) approach. Second, the parameters (phase, amplitude, and wavelength) of the coplanar and slotline modes are extracted from an amplitude modulated-like standing wave existing in the CPW feeding lines. Then a $2n \times 2n$ generalized scattering matrix of the n -port discontinuity without air bridges is derived which includes the occurring mode conversion. Finally, this generalized scattering matrix is reduced to an $n \times n$ matrix by enforcing suitable conditions at the ports which correspond to the excited slotline mode. For the purpose of illustration, the method is applied to a shielded asymmetric short-end CPW shunt stub, the scattering parameters of which are compared with those of a symmetric one. Experiments are performed on both discontinuities and the results are in good agreement with theoretical data. The advantages of using air bridges in CPW circuits as opposed to bond wires are also discussed.

I. INTRODUCTION

IN state-of-the-art MMIC's, coplanar waveguide (CPW) is becoming widely used due to several advantages it offers over the conventional microstrip line. However, air bridges are unavoidable especially when coplanar waveguide circuits are combined with other planar lines and when asymmetries in the structure give rise to the radiating slotline mode [1], [2]. Recently, transversely symmetric coplanar waveguide discontinuities with air bridges (or bond wires) have been numerically studied and the results of these studies can be found in [3]–[8]. On the other hand, some results for asymmetric CPW discontinuities with air bridges have been presented in the literature [9]–[11], but the study performed is far from complete. The full-wave FDTD method was implemented in [10] to investigate different types of CPW T-junctions, while a hybrid technique was used in [11] to analyze different asymmetric CPW discontinuities. What makes asymmetric CPW discontinuities different from symmetric ones is the presence of both the coplanar and slotline modes in the feeding lines, which necessitates the use of a special theoretical treatment to derive the scattering parameters.

Manuscript received September 30, 1992; revised March 11, 1993. This work was supported by the National Science Foundation under Contract ECS-8657951.

N. I. Dib and L. P. B. Katehi are with the Radiation Laboratory, University of Michigan, Ann Arbor, MI 48109-2122

M. Gupta is with Texas Instruments Incorporated, Dallas, TX.

G. E. Ponchak is with NASA Lewis Research Center, Cleveland, OH 44135. IEEE Log Number 9211862.

In Section II of this paper, a numerical method is presented that can be applied to characterize asymmetric CPW discontinuities. In Section IV, this method is employed to analyze a shielded asymmetric short-end CPW shunt stub. Extensive experiments on CPW shunt stubs are performed and the fabrication and measurement procedures are described in Section III. Two different approaches are used to obtain measurements of the CPW shunt stub circuits. In one approach, ground equalization is achieved using bond wires, while, in the other approach, air bridges are used. It is shown that using air bridges gives better response than bond wires.

II. THEORY

A. Application of the SDIE Method

The first step in the analysis is to derive the electric field in the slot apertures of the shielded CPW structure with the air bridges removed. The theoretical method used to study CPW discontinuities without air bridges is based on a space-domain integral equation (SDIE) which is solved using the method of moments. The SDIE approach has been previously applied to study several CPW discontinuities (without air bridges) and has shown very good accuracy, efficiency, and versatility in terms of the geometries it can solve [12]–[17]. Since the theoretical method is presented in detail in [12], [13], and [16], a brief summary will be given here.

The boundary problem pertinent to any air-bridge-free CPW discontinuity may be split into two simpler ones by introducing an equivalent magnetic current \bar{M}_s on the slot apertures. This surface magnetic current radiates an electromagnetic field in the two waveguide regions (above and below the slots) so that the continuity of the tangential electric field on the surface of the slots is satisfied. The remaining boundary condition to be applied is the continuity of the tangential magnetic field on the surface of the slot apertures, which leads to the following integral equation:

$$\hat{x} \times \int_S \int [\bar{G}_0^h(\vec{r}/\vec{r}') + \bar{G}_1^h(\vec{r}/\vec{r}')] \cdot \bar{M}_s(\vec{r}') ds' = \bar{J}_s \quad (1)$$

where $\bar{G}_{0,1}^h$ are the magnetic field dyadic Green's functions in the two waveguide regions directly above and below the slot interface, and \bar{J}_s denotes an assumed ideal electric current source exciting the coplanar waveguide structure. For a shielded CPW structure, which is the case here, the components of the dyadic Green's functions are double infinite

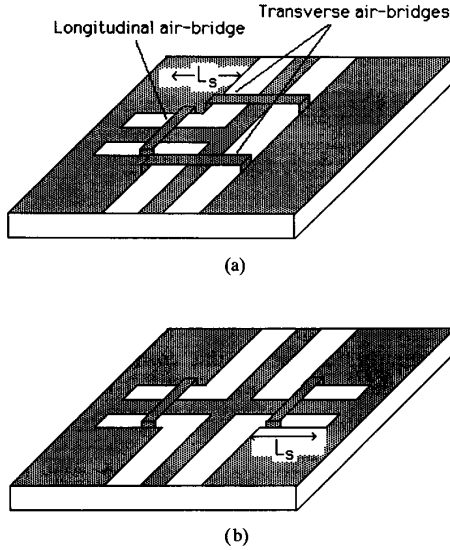


Fig. 1. (a) The asymmetric short-end CPW shunt stub. (b) The symmetric short-end CPW shunt stub.

summations over the transverse and longitudinal cavity eigenvalues.

The integral equation (1) is solved using the method of moments where the unknown magnetic current is expanded in terms of rooftop basis functions. Then, Galerkin's method is applied to reduce the above equation to a linear system of equations

$$\begin{pmatrix} Y_{yy} & Y_{yz} \\ Y_{zy} & Y_{zz} \end{pmatrix} \begin{pmatrix} V_y \\ V_z \end{pmatrix} = \begin{pmatrix} I_z \\ I_y \end{pmatrix} \quad (2)$$

where Y_{ij} ($i = y, z; j = y, z$) represent blocks of the admittance matrix, V_i is the vector of unknown y and z magnetic current amplitudes, and I_j is the excitation vector which is identically zero everywhere except at the position of the sources. Finally, the equivalent magnetic current distribution and consequently the electric field in the slots are obtained by matrix inversion.

In the case of transversely symmetric CPW discontinuities (e.g., Fig. 1(b)), the derived field in the feeding lines forms a standing wave of the fundamental coplanar mode away from the discontinuity. Consequently, the hybrid technique developed in [6]–[8] can be applied to characterize such discontinuities. However, in the case of asymmetric CPW discontinuities (e.g., Fig. 1(a)), the derived field in each slot of the feeding lines looks like an amplitude modulated signal (Fig. 2) which results from the superposition of the fundamental coplanar and slotline modes. Consequently, a special treatment is needed to separate the two modes and derive the scattering parameters of the discontinuity as described below.

B. Separation of the Two Modes

As shown in Fig. 2, the field in the feeding lines derived from the SDIE method is the superposition of the fundamental coplanar and slotline modes, each one having its own spatial parameters (wavelength, amplitude, and phase). This field is

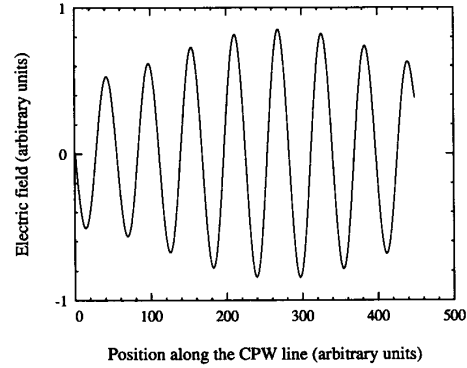


Fig. 2. A sample amplitude modulated-like standing wave existing in one of the slots of the feeding CPW which results from the superposition of the fundamental coplanar and slotline modes.

the sum of the two modes in one of the slots of the feeding CPW, and the difference between them in the other slot. To extract the parameters of each mode, one of the following methods may be used:

1) *Prony's Method*: The parameters of each mode can be obtained directly by applying Prony's method on the derived amplitude-modulated-like standing wave. Prony's method is a technique for modeling sampled data as a linear combination of exponential terms [18]. Assuming that one has N data samples of the electric field $E(1), \dots, E(N)$, Prony's method can be used to estimate $E(n)$ with a four-term complex exponential model

$$\hat{E}(n) = \sum_{k=1}^4 A_k \exp[(\alpha_k + j2\pi f_k)(n-1)T + j\theta_k] \quad (3)$$

for $1 \leq n \leq N$, where T is the sample interval, A_k is the amplitude of the complex exponential, α_k is the damping factor, f_k is the sinusoidal spatial frequency, and θ_k is the sinusoidal initial phase. A detailed description of Prony's method and a computer program listing can be found in [18]. In case of real data (lossless coplanar structures), the exponential representation reduces to

$$\hat{E}(n) = \sum_{k=c,s} 2A_k \cos[(2\pi f_k)(n-1)T + \theta_k] \quad (4)$$

for $1 \leq n \leq N$, where c and s correspond to the fundamental coplanar and slotline modes, respectively. It is found that the frequencies obtained from Prony's method agree very well with the ones predicted from a 2D program. In addition, the constructed signal is not distinguishable from the original one.

2) *The Standing-Wave Method*: In this method, the standing waves of the fundamental coplanar and slotline modes can be derived as follows:

$$V_c = \frac{V_1 - V_2}{2} \quad (5)$$

$$V_s = \frac{V_1 + V_2}{2} \quad (6)$$

where V_1 and V_2 denote the voltages in the two slots of a CPW feeding an asymmetric discontinuity. Then, the parameters

of each mode can be obtained from the position of the maxima and minima along its corresponding standing wave [16]. Alternatively, Prony's method can be applied on each single-mode standing wave to extract the parameters.

It is found that both methods give the same mode parameters with a difference of less than 0.5%. However, Prony's method has the advantage that it can be used to separate any number of modes in an overmoded structure, especially, if the number of these modes (and preferably their frequencies) is known. So, the end results of this step are the spatial parameters (wavelength, phase, and amplitude) of the fundamental coplanar and slotline modes. Consequently, the reflection coefficient and the input impedance for each mode at any point along the feeding line can be obtained.

C. The Generalized Scattering Matrix

The next step is to derive the generalized scattering matrix, which includes the interactions between the coplanar and slotline modes in the air-bridge-free asymmetric CPW discontinuity. Fig. 3 shows a generalized four-port equivalent representation of a two-port asymmetric CPW discontinuity without air bridges. This representation uses one port for each mode excited at each physical port. Thus, this four-port equivalent network takes into account the occurring mode conversion at the discontinuity. The network relations between the ports in Fig. 3 can be written as follows (see Appendix A for derivation):

$$\Gamma_{1c}(z) = S_{11} + S_{12} \frac{V_{2c}^+}{V_{1c}^+} + S_{13} \frac{V_{1s}^+}{V_{1c}^+} + S_{14} \frac{V_{2s}^+}{V_{1c}^+} \quad (7)$$

$$\Gamma_{2c}(z) = S_{21} \frac{V_{1c}^+}{V_{2c}^+} + S_{22} + S_{23} \frac{V_{1s}^+}{V_{2c}^+} + S_{24} \frac{V_{2s}^+}{V_{2c}^+} \quad (8)$$

$$\Gamma_{1s}(z) = S_{31} \frac{V_{1c}^+}{V_{1s}^+} + S_{32} \frac{V_{2c}^+}{V_{1s}^+} + S_{33} + S_{34} \frac{V_{2s}^+}{V_{1s}^+} \quad (9)$$

$$\Gamma_{2s}(z) = S_{41} \frac{V_{1c}^+}{V_{2s}^+} + S_{42} \frac{V_{2c}^+}{V_{2s}^+} + S_{43} \frac{V_{1s}^+}{V_{2s}^+} + S_{44} \quad (10)$$

where

$$V_k^+ = \frac{V_{k \max} e^{j\beta_k(z_{k \max} - z)}}{Z_{0k}(1 + |\Gamma_k|)} \quad (11)$$

In the above expressions, S_{ij} ($i, j = 1, \dots, 4$) are the unknown components of the generalized scattering matrix, $V_{k \max}$ and $z_{k \max}$ are the value and position of a voltage maximum along the k th port, and β_k is the propagation constant at the k th port. In addition, Γ_k is the reflection coefficient at the reference plane z of port k , the magnitude of which ($|\Gamma_k|$) is equal to one for a shielded structure. Moreover, Z_{0k} is the characteristic impedance of the transmission line connected to the k th port which is obtained using a 2D program. In general, four independent excitations are needed to evaluate the 16 unknown components of the generalized scattering matrix.

D. The 2×2 Scattering Matrix

The 4×4 generalized scattering matrix derived above includes the interactions between the coplanar and slotline

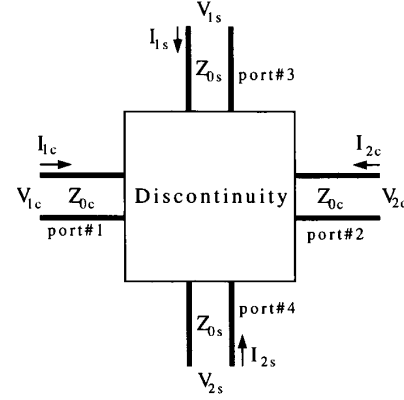


Fig. 3. A generalized four-port equivalent representation of a two-port CPW asymmetric discontinuity without air bridges where the fundamental coplanar and slotline modes are excited.

modes in the air-bridge-free CPW discontinuity. However, in practice, the slotline mode is always suppressed by connecting the two ground planes of the feeding lines with air bridges. These transverse air bridges can be taken into account by connecting a parallel LC combination to the ports corresponding to the slotline mode, while connecting a series LC combination to those corresponding to the coplanar mode. These inductor and capacitor are due to the parasitic effects of the transverse air bridges, which can be evaluated quasi-statically by modeling the air bridge either as an air-filled microstrip line or a parallel-plate waveguide [6]–[8]. However, for typical air bridges, these connections effectively short the slotline mode ports and leave the coplanar mode ports unaffected. Thus, the presence of the transverse air bridges can be modeled numerically by imposing the following two conditions on the network shown in Fig. 3:

$$V_{1s} = 0 \quad (12)$$

$$V_{2s} = 0 \quad (13)$$

It should be noted that such conditions apply to typical air bridges, the parasitic effects of which have been found to be negligible [1], [2], [4], [5]. Hence, transverse air bridges placed at the reference planes of the generalized scattering matrix reduce the four-port network representation to a two-port one. This, in effect, gives a 2×2 scattering matrix which describes the discontinuity under coplanar mode excitation only. It can be easily shown (see Appendix B) that the elements of this 2×2 scattering matrix are related to those of the 4×4 generalized scattering matrix as follows:

$$S'_{11} = S_{11} - S_{13}A - S_{14}B \quad (14)$$

$$S'_{12} = S'_{21} = S_{12} - S_{13}B - S_{14}A \quad (15)$$

$$S'_{22} = S_{22} - S_{23}B - S_{24}A \quad (16)$$

where

$$A = \frac{S_{31}(1 + S_{44}) - S_{41}S_{34}}{(1 + S_{33})(1 + S_{44}) - S_{34}S_{43}} \quad (17)$$

$$B = \frac{S_{41}(1 + S_{33}) - S_{43}S_{31}}{(1 + S_{33})(1 + S_{44}) - S_{34}S_{43}} \quad (18)$$

and S'_{ij} are the components of the 2×2 scattering matrix.

III. FABRICATION AND MEASUREMENTS

Two different approaches are used to obtain measurements of the shunt stub circuits shown in Fig. 1. In the first approach, ground equalization is achieved using bond wires, while, in the second the ground planes are connected with air bridges.

A. Circuits with Bond Wires

A 300-Å seed layer of Cr and a 600-Å layer of Au is evaporated on a 3-inch high-resistivity silicon wafer. This metallization provides the electrical contact for the electroplating. A photolithographic process is then used to define the various shunt stub geometries and the plating contact area. Approximately $3 \mu\text{m}$ of gold is electroplated to achieve the required number of skin depths, then, bond wires are added to the circuits using a Marpet Enterprises wire bonder and 0.7-mil-thick gold thread.

B. Circuits with Air Bridges

In this case, the circuits are fabricated on a 483- μm -thick GaAs substrate using a lift-off processing technique. The CPW center strip and ground planes consist of 200 Å of Cr and $1.5 \mu\text{m}$ of Au. The air bridges have 15- μm -square posts and a height and width of 3.5 and $15 \mu\text{m}$, respectively. The bridge itself is $1.5 \mu\text{m}$ thick and was fabricated by lift-off.

C. Measurements

All of the circuits are measured with a probe station and Cascade Microtech high-frequency CPW probes attached to an HP 8510B Network Analyzer. To suppress parallel-plate and microstrip modes between the CPW circuits and the wafer chuck of the probe station during testing, the wafer is placed on a piece of 0.125-inch-thick 5880 RT/Duriod. A thru-reflect-line (TRL) calibration is performed to eliminate the effects of the connectors, cables, and probes from the measured data and to accurately place the system reference planes at the reference planes of the stubs. The calibration standards required for the TRL include a thru, an open, and several delay lines. Three delay lines are used in the calibration of the circuits with air bridges to cover the full 5–40 GHz bandwidth, whereas only one delay line is used in the case of the circuits with bond wires to cover a 10–30 GHz bandwidth. After calibrating, S -parameters measurements of the circuits are used to compare the theoretical and experimental results.

IV. RESULTS AND DISCUSSION

The theoretical technique described in Section II is quite general so that it can be applied to any n -port CPW discontinuity. The method is employed here to analyze the asymmetric short-end CPW shunt stub shown in Fig. 1(a). Since this discontinuity involves a longitudinal air bridge that connects the two ground planes of the CPW stub, one more step is required after the evaluation of the 2×2 scattering matrix. First, a two-port lumped-element equivalent circuit is derived from this 2×2 scattering matrix. Then, this circuit is modified

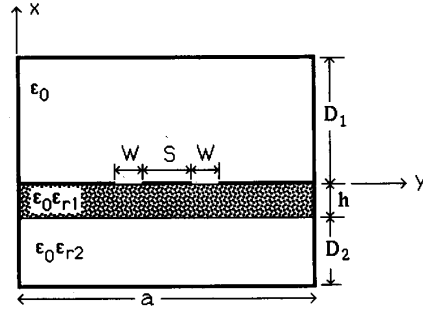


Fig. 4. A suspended CPW structure inside a rectangular cavity.

by incorporating the longitudinal air bridge from which the new scattering parameters can be obtained (see [6]–[8] for details). The scattering parameters of this asymmetric stub discontinuity will be compared to those of a symmetric short-end CPW shunt stub shown in Fig. 1(b).

Three examples are presented in this section. In the first example, an asymmetric stub is analyzed theoretically and is compared to a symmetric stub with the same dimensions. In the second example, experimental results obtained from the circuits with bond wires are compared to theoretical data. In the last example, experimental results for the circuits with air bridges are compared to theoretical data and the radiation loss from the stubs is experimentally investigated.

A. Example 1: Comparison Between Asymmetric and Symmetric Stubs

In the numerical results shown in Figs. 5 through 9, the considered CPW discontinuities are suspended inside a rectangular cavity, as shown in Fig. 4, with $h = 400 \mu\text{m}$, $\epsilon_{r1} = 13$, $\epsilon_{r2} = 1$, $S = 75 \mu\text{m}$, $W = 50 \mu\text{m}$, $a = 3.425 \text{ mm}$, and $D_1 = D_2 = 1.2 \text{ mm}$. On the other hand, the CPW stubs are placed at the center of the cavity with a slot width of $25 \mu\text{m}$ and a center conductor of $25 \mu\text{m}$.

Figs. 5 and 6 show the elements of the first and third rows of the 4×4 generalized scattering matrix of an air-bridge-free asymmetric short-end stub. Other elements can be obtained using symmetry considerations, e.g., $S_{21} = S_{12}$, $S_{22} = S_{11}$, $S_{23} = S_{14}$, etc. It should be noted here that ports #1 and #2 correspond to the coplanar mode at the first and second physical ports, respectively, while ports #3 and #4 correspond to the slotline mode (see Fig. 3). Thus, it can be noticed from the values of S_{12} in Fig. 5 that if one of the physical ports is excited by a coplanar mode, 50–65% of the power is transmitted to the coplanar mode appearing on the other physical port in the whole frequency range. On the other hand, S_{13} shows that 15–20% of the input power is transferred to the slotline mode appearing on the same physical port. It is interesting to note that at 27 GHz the amount of power in the slotline mode appearing at both ports is the same and that the return loss (S_{11}) reaches its minimum value. In addition, it can be noticed from the values of S_{34} in Fig. 6 that if one of the physical ports is excited by a slotline mode, the power transmitted to the slotline mode on the other port decreases as the frequency increases until it reaches a minimum value at

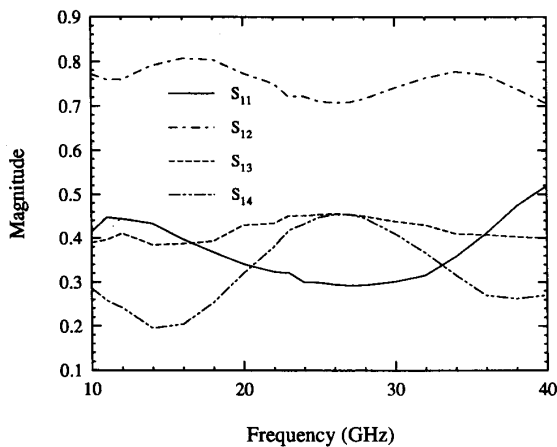


Fig. 5. Elements of the first row of the generalized scattering matrix of an air-bridge-free asymmetric short-end CPW shunt stub. ($L_s = 1100 \mu\text{m}$).

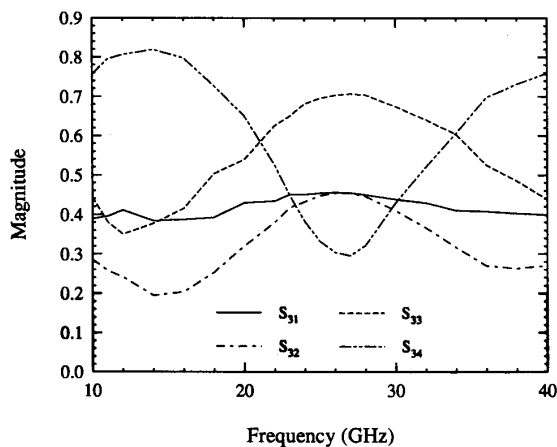


Fig. 6. Elements of the third row of the generalized scattering matrix of an air-bridge-free asymmetric short-end CPW shunt stub. ($L_s = 1100 \mu\text{m}$).

27 GHz after which it increases with frequency. The opposite happens for the amount of power carried by the reflected slotline mode on the same input port as depicted from S_{33} .

Fig. 7 shows the scattering parameters of the same asymmetric stub discontinuity after taking the transverse air bridges into consideration. In addition, the scattering parameters of a symmetric stub discontinuity (with the same dimensions) without air bridges are plotted in the same figure. It can be noticed that both structures exhibit totally different characteristics when the longitudinal air bridges are removed. It is interesting to observe that the asymmetric stub without the longitudinal air bridges still behaves as a shunt stub resonating at approximately 27 GHz. However, this frequency is not the expected resonant frequency of the coplanar mode in the stub (see Fig. 8). On the other hand, the behavior of the symmetric stub without the longitudinal air bridges is far from being a shunt stub [6]–[8].

Fig. 8 shows the scattering parameters of both discontinuities with all air bridges taken into consideration.

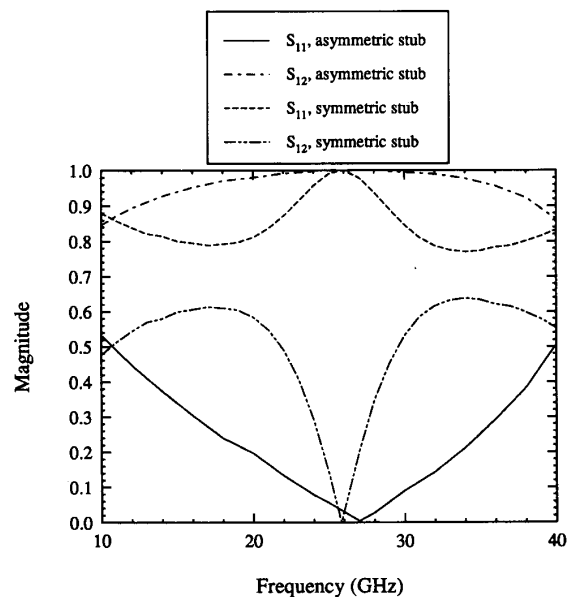


Fig. 7. Scattering parameters of both the symmetric and asymmetric short-end CPW shunt stub discontinuities without longitudinal air bridges. ($L_s = 1100 \mu\text{m}$).

The width and height of the longitudinal air bridge are assumed to be 15 and $3 \mu\text{m}$, respectively. It is seen now that indeed both the asymmetric and symmetric structures behave as short-end shunt stubs with resonant frequencies of approximately 24.5 and 25.2 GHz, respectively. The difference in the resonant frequencies can be attributed to the asymmetry in one of the discontinuities. It is also interesting to note that the symmetric stub has a higher Q than the asymmetric stub. The difference between the resonant frequencies of an asymmetric stub with and without the longitudinal air bridge (as seen in Figs. 7 and 8) decreases if a substrate with higher dielectric constant and/or smaller stub dimensions (slot and center conductor widths) is chosen, as will be shown in Example 3. This is due to the fact that for a CPW with very small S and W and/or large ϵ_r , the propagation constants of the slotline mode and the coplanar mode become approximately equal as the frequency increases [19].

Fig. 9 shows the phase of the scattering parameters of both discontinuities with all air bridges taken into consideration. The similarity between the two types of shunt CPW stubs when all air bridges are present is clearly seen.

B. Example 2: Stubs with Bond Wires

A comparison between theoretical and experimental results for an asymmetric stub discontinuity without longitudinal air bridge is shown in Fig. 10. For this structure, $h = 353 \mu\text{m}$, $\epsilon_{r1} = 11.7$, $\epsilon_{r2} = 1$, $S = 140 \mu\text{m}$, $W = 100 \mu\text{m}$, $a = 4.56 \text{ mm}$, $D_1 = 3.5 \text{ mm}$, and $D_2 = 1.8 \text{ mm}$. In addition, the CPW stub has a slot width of $100 \mu\text{m}$ and a center conductor of $140 \mu\text{m}$. The measurements were done on unshielded structures and bond wires were used to connect

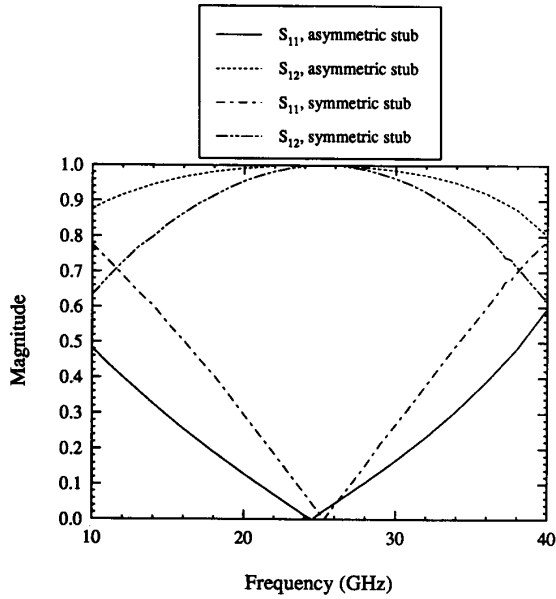


Fig. 8. Scattering parameters of both the symmetric and asymmetric short-end CPW shunt stub discontinuities with all air bridges. ($L_s = 1100 \mu\text{m}$).

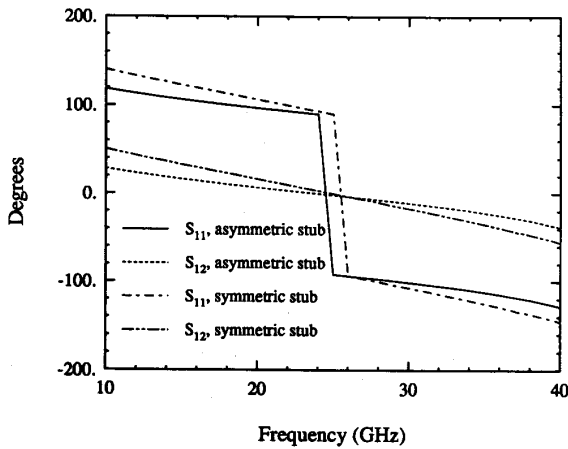


Fig. 9. The phase of the scattering parameters of the symmetric and asymmetric short-end CPW shunt stub discontinuities with all air bridges taken into consideration. The reference planes are taken at the end of the uniform coplanar lines. ($L_s = 1100 \mu\text{m}$).

the ground planes, as was discussed in the previous section. In Fig. 10, the discrepancy between theory and experiment is due to radiation loss from the measured stub and the fact that bond wires are not very effective in suppressing the slotline mode. It should be mentioned here that in the measured stub, the transverse bond wires, which connect the ground planes of the feeding lines, were placed at a distance of $90 \mu\text{m}$ from the junction. However, the theoretical methodology assumes that ideal transverse air bridges exist exactly at the junction.

Fig. 11 shows the scattering parameters (theoretical and experimental) of the same asymmetric stub after including the longitudinal bond wire in the experiments and taking the

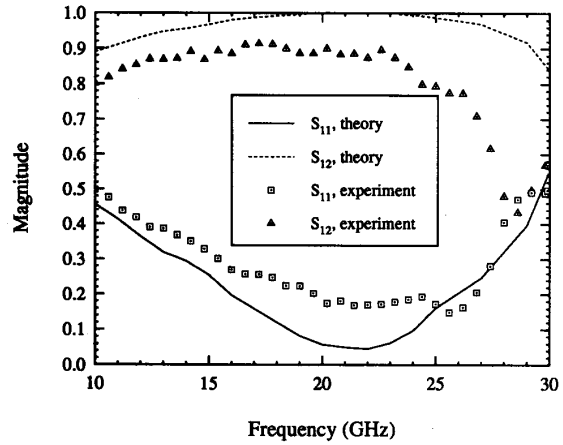


Fig. 10. Scattering parameters of an asymmetric short-end shunt CPW stub without longitudinal air bridge. ($L_s = 1600 \mu\text{m}$).

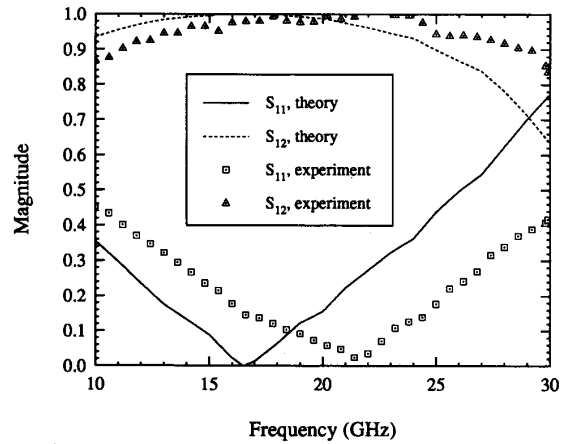


Fig. 11. Scattering parameters of an asymmetric short-end shunt CPW stub with longitudinal air bridge. ($L_s = 1600 \mu\text{m}$).

longitudinal air bridge into consideration in the theory. The air bridge is assumed to be of height $3 \mu\text{m}$. In this figure, the overall agreement between theory and experiment is better than that in Fig. 10. This is due to the fact that the longitudinal bond wire tends to suppress the radiating slotline mode in the measured stub. The difference in the resonant frequency can be attributed to the fact that the longitudinal bond wire, which connects the stub ground planes, was placed at a distance of $190 \mu\text{m}$ from the junction. This reduces the effective length of the stub, and thus increases the measured resonant frequency. On the other hand, the derived theoretical data for this discontinuity are based on the assumption that a longitudinal air bridge is placed exactly at the junction. Another reason for the discrepancy in the resonant frequency is the relatively thick metallization used in the circuits with bond wires ($3 \mu\text{m}$), which is neglected in the theoretical analysis. The finite metallization thickness reduces the phase constant [20], and thus increases the stub resonant frequency [8].

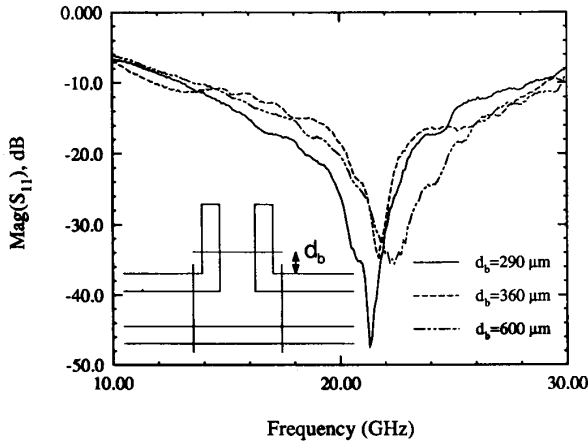
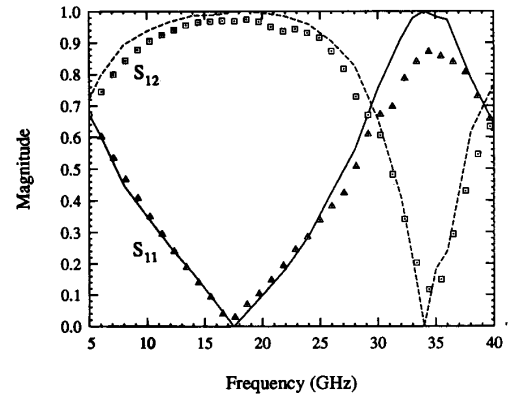


Fig. 12. Measured $\text{Mag}(S_{11})$ for an asymmetric CPW shunt stub for different longitudinal bond-wire positions. ($L_s = 1600 \mu\text{m}$).

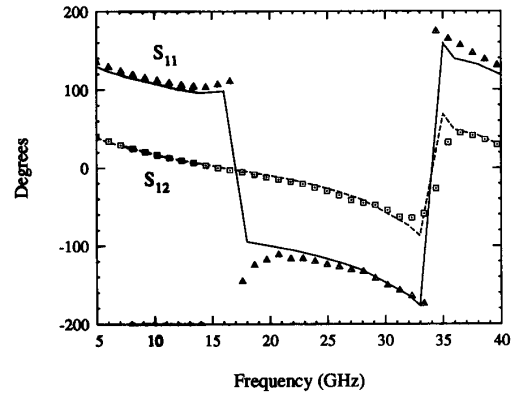
Fig. 12 shows the measured S_{11} of the asymmetric stub with three different longitudinal bond-wire positions. The bond wires could not be placed exactly at the junction due to the physical limitations of the wire bonder. Fig. 12 shows that the resonant frequency of the considered asymmetric CPW shunt stub is relatively insensitive to the position of the longitudinal bond wire for $d_b \geq 290 \mu\text{m}$. On the other hand, it has been found experimentally that the position of the bond wires has a more pronounced effect on the resonant frequency of a symmetric CPW shunt stub.

C. Example 3: Stubs with Air Bridges

Figs. 13 and 14 show the scattering parameters (theoretical and experimental) of an asymmetric stub with and without longitudinal air bridge. For this structure, $h = 483 \mu\text{m}$, $\epsilon_{r1} = 13$, $\epsilon_{r2} = 1$, $S = 32 \mu\text{m}$, $W = 20 \mu\text{m}$, $a = 4.318 \text{ mm}$, $D_1 = 3.0 \text{ mm}$, and $D_2 = 3.175 \text{ mm}$. In addition, the CPW stub has a slot width of $15 \mu\text{m}$ and a center conductor of $20 \mu\text{m}$. The measurements were performed on unshielded structures and air bridges were used to connect the ground planes. As opposed to bond wires, the air bridges were placed at the junction exactly. The agreement between theory and experiment is very good, which validates both sets of data. The discrepancy seen around the second resonance is mainly due to radiation losses. It is interesting to note that the behavior of the stub with and without the longitudinal air bridge is almost the same. The resonant frequencies shown in Fig. 13 and 14 differ only by almost 0.8 GHz. The reason is that the dimensions of the stub (slot and center conductor widths) are very small, and thus, the transverse air bridges tend to equalize the potential of the two ground planes of the stub as well as the ground planes of the feeding lines. In addition, as mentioned earlier, the propagation constants of the slotline and coplanar modes are approximately the same for the CPW under consideration. Specifically, β_c/β_0 equals 2.64 and β_s/β_0 equals 2.4 at 18 GHz, where β_c , β_s , and β_0 are the coplanar-mode, slotline-mode, and free-space propagation constants, respectively. A symmetric CPW stub



(a)



(b)

Fig. 13. Scattering parameters of an asymmetric CPW shunt stub without longitudinal air bridge. Straight lines: theory, symbols: experiment. ($L_s = 1650 \mu\text{m}$).

with the same dimensions has also been measured and found to have a higher Q factor and a somewhat larger resonant frequency than the asymmetric stub, which conforms with what was found theoretically in Example 1.

Fig. 15 shows the measured loss factor for both the symmetric and asymmetric CPW shunt stubs with all air bridges present. It can be seen that the higher Q which has been observed for the symmetric case is not due to lower losses but rather due to the fact that the amount of energy stored in the symmetric stub is larger than that stored in the asymmetric one. It can be also observed that the loss factor for the symmetric stub increases with frequency at nearly linear rate, whereas the loss factor for the asymmetric stub decreases to a minimum at the first resonant frequency and then passes to a maximum at the second resonant frequency where the stub is half a wavelength long. This increase in the loss factor at the second resonance is due to the radiation loss attributed to the slotline mode. It seems that the slotline mode is not excited as strongly in the symmetric stub and, thus, there is no corresponding increase in radiation loss at the second resonance. The decrease in the loss factor for the asymmetric stub at the first resonance has been confirmed by repeated measurements.

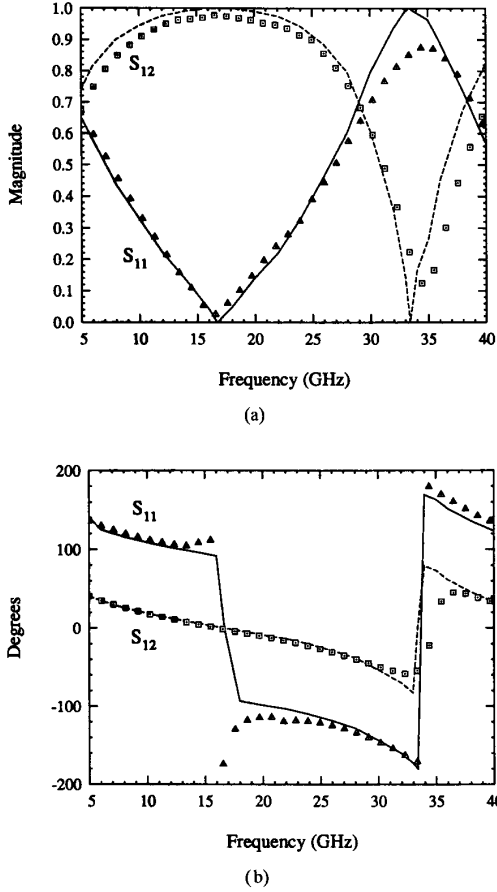


Fig. 14. Scattering parameters of an asymmetric CPW shunt stub with longitudinal air bridge. Straight lines: theory, symbols: experiment. ($L_s = 1650 \mu\text{m}$).

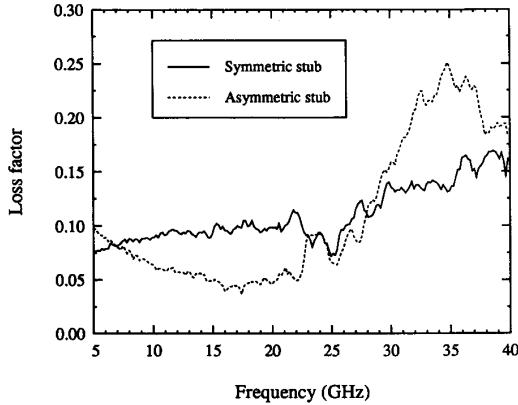


Fig. 15. Measured loss factor for both the symmetric and asymmetric CPW shunt stubs with all air bridges present. ($L_s = 1650 \mu\text{m}$).

V. CONCLUSIONS

A general technique to characterize asymmetric CPW discontinuities, where both the fundamental coplanar and slotline modes may be excited, has been developed. First, the planar

structure with the air bridges removed is analyzed using the SDIE method, which results in an amplitude modulated-like standing wave pattern in the feeding CPW lines. Second, the two modes forming such a standing wave are separated by either using Prony's method or the standing-wave method. Third a $2n \times 2n$ generalized scattering matrix is obtained, which includes the occurring mode conversion due to the discontinuity. Finally, this matrix is reduced to an $n \times n$ scattering matrix by forcing the slotline mode voltages at the corresponding ports to be zero. This approach has been applied to the asymmetric short-end CPW shunt stub. The scattering parameters of this discontinuity have been compared to those of a symmetric short-end CPW shunt stub. It has been found that the symmetric stub has a higher Q than the asymmetric stub with the same dimensions. Extensive experiments have been performed on CPW circuits with bond wires and air bridges. The circuits with bond wires are much easier to fabricate but some of the accuracy is sacrificed. Air bridges provide much more accuracy in the measurements, though they are more difficult to fabricate.

APPENDIX A

In this appendix, (7)–(11) are derived. The voltage at any point along a transmission line (connected to port k) can be expressed in terms of forward and backward traveling waves as follows:

$$V_k(z) = V_k^+ e^{-j\beta_k z} + V_k^- e^{j\beta_k z}. \quad (\text{A1})$$

The above equation may be written as

$$V_k(z) = V_k^+ e^{-j\beta_k z} (1 + \Gamma_k(z)) \quad (\text{A2})$$

where $\Gamma_k(z)$ is the reflection coefficient at the point z along the line. Using the fact that the angle of this reflection coefficient is zero at a voltage maximum, V_k^+ may be written as

$$V_k^+ = \frac{V_{k_{\max}} e^{j\beta_k z_{k_{\max}}}}{1 + |\Gamma_k|} \quad (\text{A3})$$

where $V_{k_{\max}}$ is the complex value of the voltage maximum, $z_{k_{\max}}$ is its position along the line and β_k is the propagation constant.

Now, the network relations between the four ports of the generalized representation shown in Fig. 3 may be written as follows:

$$\begin{bmatrix} b_{1c} \\ b_{2c} \\ b_{1s} \\ b_{2s} \end{bmatrix} = \begin{bmatrix} S_{11} & S_{12} & S_{13} & S_{14} \\ S_{21} & S_{22} & S_{23} & S_{24} \\ S_{31} & S_{32} & S_{33} & S_{34} \\ S_{41} & S_{42} & S_{43} & S_{44} \end{bmatrix} \begin{bmatrix} a_{1c} \\ a_{2c} \\ a_{1s} \\ a_{2s} \end{bmatrix}. \quad (\text{A4})$$

In the above, a_k and b_k are defined as

$$a_k = \frac{V_k^+ e^{-j\beta_k z}}{\sqrt{Z_{0k}}} \quad (\text{A5})$$

$$b_k = \frac{V_k^- e^{j\beta_k z}}{\sqrt{Z_{0k}}} \quad (\text{A6})$$

where Z_{0k} is the characteristic impedance of the connecting line at port k . Substituting (A5) and (A6) in (A4) and using (A3), it is straightforward to derive (7)–(11).

APPENDIX B

In this appendix, the derivation of (14)–(18) is outlined. First, the following conditions are enforced on the generalized network shown in Fig. 3:

$$V_{1s} = 0 \quad (\text{B1})$$

$$V_{2s} = 0. \quad (\text{B2})$$

The above conditions lead to the following relations between the incident and reflected waves on the ports corresponding to the slotline mode:

$$a_{1s} = -b_{1s} \quad (\text{B3})$$

$$a_{2s} = -b_{2s}. \quad (\text{B4})$$

Using (B3) and (B4), (A4) may be written as

$$\begin{bmatrix} b_{1c} \\ b_{2c} \\ b_{1s} \\ b_{2s} \end{bmatrix} = \begin{bmatrix} S_{11} & S_{12} & S_{13} & S_{14} \\ S_{21} & S_{22} & S_{23} & S_{24} \\ S_{31} & S_{32} & S_{33} & S_{34} \\ S_{41} & S_{42} & S_{43} & S_{44} \end{bmatrix} \begin{bmatrix} a_{1c} \\ a_{2c} \\ -b_{1s} \\ -b_{2s} \end{bmatrix}. \quad (\text{B5})$$

Using the third and fourth equations of the above system, one can derive expressions for b_{1s} and b_{2s} in terms of a_{1c} and a_{2c} . Finally, substituting these expressions in the first and second equations of (B5), (14)–(18) can be obtained.

ACKNOWLEDGMENT

One of the authors (N.D.) wishes to thank Prof. Emad Ebbini for the useful discussions on the use of Prony's method.

REFERENCES

- [1] N. Koster *et al.*, "Investigation of air bridges used for MMICs in CPW technique," in *Proc. 19th European Microwave Conf.*, Sept. 1989, pp. 666–671.
- [2] T. Hirota, Y. Tarusawa, and H. Ogawa, "Uniplanar MMIC hybrids—A proposal of a new MMIC structure," *IEEE Trans. Microwave Theory Tech.*, vol. MTT-35, pp. 576–581, June 1987.
- [3] M. Rittweger, M. Abdo, and I. Wolff, "Full-wave analysis of coplanar discontinuities considering three-dimensional bond wires," in *1991 IEEE MTT-S Int. Microwave Symp. Dig.*, pp. 465–468.
- [4] K. Beilenhoff, W. Heinrich, and H. Hartnagel, "The scattering behavior of air bridges in coplanar MMIC's," in *Proc. 21st European Microwave Conf.*, Sept. 1991, pp. 1131–1135.
- [5] H. Jin and R. Vahldieck, "Calculation of frequency-dependent S-parameters of CPW air-bridges considering finite metallization thickness and conductivity," in *1992 IEEE MTT-S Int. Microwave Symp. Dig.*, pp. 207–210.
- [6] N. Dib, L. P. Katehi, and G. Ponchak, "Analysis of shielded CPW discontinuities with air bridges," in *1991 IEEE MTT-S Int. Microwave Symp. Dig.*, pp. 469–472.
- [7] ———, "A comprehensive theoretical and experimental study of CPW shunt stubs," *1992 IEEE MTT-S Int. Microwave Symp. Dig.*, pp. 947–950.
- [8] ———, "A theoretical and experimental study of CPW shunt stubs," *IEEE Trans. Microwave Theory and Tech.*, pp. 38–44, Jan. 1993.
- [9] R. E. Stegens, "Coplanar waveguide FET amplifiers for satellite communications systems," *Comsat Tech. Rev.*, vol. 9, pp. 255–267, Spring 1979.
- [10] M. Rittweger *et al.*, "Full-wave analysis of a modified coplanar air bridge T-junction," in *Proc. 21st European Microwave Conf.*, Sept. 1991, pp. 993–998.
- [11] R. Bromme and R. Jansen, "Systematic investigation of coplanar waveguide MIC/MMIC structures using a unified strip/slot 3D electromagnetic simulator," in *1991 IEEE MTT-S Int. Microwave Symp. Dig.*, pp. 1081–1084.
- [12] N. Dib and L. P. Katehi, "Modeling of shielded CPW discontinuities using the space domain integral equation method (SDIE)," *J. Electromagnetic Waves and Applications*, vol. 5, nos. 4/5, pp. 503–523, 1991.
- [13] N. Dib, L. P. Katehi, G. Ponchak, and R. Simons, "Theoretical and experimental characterization of coplanar waveguide discontinuities for filter applications," *IEEE Trans. Microwave Theory Tech.*, vol. 39, pp. 873–882, May 1991.
- [14] N. Dib and L. P. Katehi, "The effect of mitering on CPW discontinuities," in *Proc. 21st European Microwave Conf.*, Sept. 1991, pp. 223–228.
- [15] N. Dib, W. Harokopus, G. Ponchak, and L. P. Katehi, "A comparative study between shielded and open coplanar waveguide discontinuities," *Int. J. Microwave and MM-Wave Computer Aided Eng.*, vol. 2, no. 4, pp. 331–341, Oct. 1992.
- [16] N. Dib, "Theoretical characterization of coplanar waveguide transmission lines and discontinuities," Ph.D. dissertation, Univ. of Michigan, Ann Arbor, 1992.
- [17] W. Harokopus and L. P. Katehi, "Radiation loss from open coplanar waveguide discontinuities," in *1991 IEEE MTT-S Int. Microwave Symp. Dig.*, pp. 743–746.
- [18] S. Marple, Jr., *Digital Spectral Analysis with Applications*. Englewood Cliffs, NJ: Prentice-Hall, 1987.
- [19] R. Simons, "Suspended coupled slotline using double layer dielectric," *IEEE Trans. Microwave Theory Tech.*, vol. MTT-29, pp. 162–165, Feb. 1981.
- [20] K. Koshiji, E. Shu, and S. Miki, "An analysis of coplanar waveguide with finite conductor thickness—Computation and measurement of characteristic impedance," *Electron. Commun. Japan*, vol. 64-B, no. 8, pp. 69–78, 1981.



Nihad Dib (S'89–M'92) received the B.Sc. degrees in electrical engineering from Kuwait University in 1985 and 1987, respectively, and the Ph.D. degree in electrical engineering from the University of Michigan, Ann Arbor, in 1992.

He is currently working as an Assistant Research Scientist at the Radiation Laboratory at the University of Michigan, Ann Arbor. His current research interests include the numerical analysis and modeling of planar discontinuities and dielectric lines.

Dr. Dib was a recipient of a Pre-Doctoral Rackham Fellowship, University of Michigan, during the academic year 1991–1992.



Mino Gupta received the B.S.E.E. and M.S. degrees in electrical engineering from the University of Michigan, Ann Arbor, in 1991 and 1992, respectively.

She is currently employed by Texas Instruments Incorporated, Dallas, TX, in the Defense Systems and Electronics Group in the Microwave Engineering Division.



George E. Ponchak (S'82–M'93) received the B.E.E.E. degree from Cleveland State University, Cleveland, OH, in 1983 and the M.S.E.E. degree from Case Western Reserve University, Cleveland, OH, in 1987. He is currently pursuing the Ph.D. degree from the University of Michigan.

He joined the Space Electronics Division of NASA Lewis Research Center, Cleveland, OH, in 1983. Since joining NASA, he has been responsible for research of microwave and millimeter-wave transmission lines and passive elements with a

primary emphasis on coplanar waveguide. In addition, he has been responsible for the management of several monolithic microwave integrated circuit (MMIC's) contracts.



Linda P. B. Katehi (S'81–M'84–SM'89) received the B.S.E.E degree from the National Technical University of Athens, Greece, in 1977 and the M.S.E.E. and Ph.D. degrees from the University of California, Los Angeles, in 1981 and 1984, respectively.

In September 1984 she joined the faculty of the EECS Department of the University of Michigan, Ann Arbor. Since then she has been involved in the modeling and computer-aided design of millimeter- and near-millimeter-wave monolithic circuits and

In 1984 she received the W. P. King Award and in 1985 the S. A. Schelkunoff Award from the Antennas and Propagation Society. In 1987 she received an NSF Presidential Young Investigator Award and an URSI Young Scientist Fellowship. She is a member of the IEEE AP-S and MTT-S, Sigma Xi, and URSI Commission D.

antennas.